Integer and fractional quantum hall effects in lattice magnets

Venderbos, J.W.F.

CHAPTER 3

THE HONEYCOMB LATTICE MAGNET

3.1 Introduction

The physics of the KLM on non-frustrated lattices, such as the square and cubic one, has been studied extensively. In particular the limit of strong coupling and large localized moments, where the KLM goes over into the double-exchange (DE) model, is directly relevant to the colossal magnetoresistance effect in perovskite manganites [28,41–45]. In such cases, the competition between DE and antiferromagnetic (AFM) superexchange can lead to canted spin states or phase separation [28]. Although the honeycomb lattice is also bi-partite, it has the smallest possible coordination number for proper 2D lattices. That the honeycomb lattice can support physical phenomena fundamentally different from square lattices, is illustrated by recent Quantum Monte Carlo calculations [46], which identify a novel spin-liquid phase for the Hubbard model on the honeycomb lattice, a finding supported by analytical studies [47–49].

In this chapter, we investigate the consequences of the competition between AFM superexchange and ferromagnetic (FM) DE on the honeycomb lattice. We find that two exotic ground states exist between the trivial, fully FM and AFM phases. In the first, nearer to the FM state, the spins self-organize into FM hexagons that are coupled antiferromagnetically. Since the hexagonal rings form a *frustrated* triangular lattice, their order is reminiscent of the Yafet-Kittel state [50]. The competition between

isotropic magnetic interactions thus causes geometric frustration to emerge in a non-frustrated lattice.

For slightly stronger AFM interactions, we find the *exact* groundstate to consist of independent FM dimers containing one electron each. Apart from the requirement that the alignment of adjacent dimers be AFM, they are independent. The groundstate of this N-spin system therefore has a high degeneracy $\propto 2^{\sqrt{N}}$. While the macroscopic degeneracy $\propto e^{\alpha N}$ in (spin) ice is caused by the local symmetry of the frustrated tetrahedra [51, 52], our $\sqrt{N}$ exponent indicates the presence of an 'intermediate' symmetry – a symmetry between local and global [53]. It is remarkable that this highly degenerate groundstate manifold arises as an *emergent* effect in a Hamiltonian that itself does not have such a symmetry.

In many materials, the essence of the electronic structure is captured by interacting spins and electrons on a honeycomb lattice. Interactions between impurity magnetic moments on the honeycomb lattice of graphene have been intensely studied in a Ruderman-Kittel-Kasuya-Yosida (RKKY) framework [54–56] and using the KLM [57]. Going beyond RKKY is even more important in transition metal oxides, e.g., $Bi_3Mn_4O_{12}(NO_3)$ [58–62] or Li_2MnO_3 [63], with Mn ions on a honeycomb lattice.

3.2 Model and method

The Hamiltonian corresponding to the one-band DE model in the presence of competing AFM superexchange interactions on a honeycomb lattice is

$$H = -\sum_{\langle ij\rangle} t_{ij}(\hat{\psi}_i^\dagger \hat{\psi}_j + H.c.) + J_{\mathrm{AF}} \sum_{\langle ij\rangle} \vec{S}_i \cdot \vec{S}_j, \tag{3.1}$$

where $\hat{\psi}_i^\dagger$ and $\hat{\psi}_i$ are the fermionic creation and annihilation operators, respectively. In accordance with the DE scheme these fermions have their spin aligned with the on-site spins $\vec{S}_i$. The on-site core spins are treated as classical spins with $|\vec{S}_i| = 1$ and thus can be specified by their polar and azimuthal angles (θ_i, ϕ_i). Both sums are over nearest neighbors. Due to the alignment of electron spin to the core spins, the hopping amplitude depends on the direction of the core spins, $t_{ij} = t_0[\cos(\theta_i/2)\cos(\theta_j/2) + \sin(\theta_i/2)\sin(\theta_j/2)e^{-i(\phi_i-\phi_j)}]$ [28]. The strength of the AFM super-exchange is given by J_{AF} and all energies are in units of the hopping amplitude t_0. To guarantee an unbiased search for groundstate candidates, we employ a well-established hybrid method of exact diagonalization (ED) for the bilinear fermionic part of the Hamiltonian and Monte Carlo (MC) for the classical spins [28]. Each MC configuration is defined by a given core spin texture and Markov chains are generated by

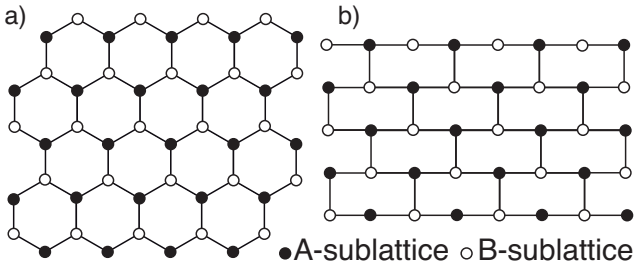

Figure 3.1: Schematic view of (a) the honeycomb lattice and (b) the brick-wall lattice having the same topology.

diagonalizing the fermionic problem for each configuration update. We also make use of the travelling cluster approximation (TCA), which has proven its validity and success in earlier studies on a similar class of models [43–45], to go to larger lattice sizes. We report here results based on calculations on an $N = 12^2$ honeycomb lattice, using a cluster of size $N_c = 6^2$. In the MC routine we use $\sim 10^4$ steps for equilibration and the same number of steps for thermal averaging. We focus on the case of a half-filled band, which refers to 1/2 an electron per site, equivalent to quarter-filling in the spinful problem. For selected parameter values, the MC procedure was further refined by an optimization routine that diminishes thermal fluctuations [64].

To identify the magnetically ordered states, we calculate the spin structure factor

$$S(\vec{q}) = \frac{1}{4N^2} \sum_{i,j} \langle \vec{S}_i \cdot \vec{S}_j \rangle e^{i\vec{q}\cdot(\vec{r}_i - \vec{r}_j)}, \tag{3.2}$$

where $\langle \ldots \rangle$ is a thermal average and $\vec{r}_i$ is the position space vector of site i. For a clear understanding of the real-space structure of the magnetic states it is helpful to look at $S(\vec{q})$ on a square geometry [see Fig. 3.1(b)]. A specific long-range ordering is expressed as the point in the Brillouin zone where the structure factor shows a peak. To analyze the electronic properties we compute the density of states (DOS) as $D(\omega) = \langle \frac{1}{N} \sum_k \delta(\omega - \epsilon_k) \rangle$ and approximate the delta-function by a Lorentzian with broadening γ.

3.3 Results

In the absence of super-exchange interaction ($J_{\mathrm{AF}} = 0$), the spins order ferromagnetically, as expected from the DE mechanism. The fermionic problem is then equivalent

to non-interacting spinless electrons on a honeycomb lattice, giving rise to a dispersion and DOS that is well-known from graphene [see Fig. 4.2(a)]. Introducing a small J_{AF} still leads to a FM ground state. At $J_{AF} \approx 0.14$, the FM state becomes unstable and gives way to a state with $S(\vec{q})$ peaked at $\frac{2}{3}(\pi, 0)$ (and the points related to it by symmetry). and with the peculiar four-peak DOS shown in Fig. 4.2(b). Real-space snapshots show that a superlattice formed of hexagons emerges at low temperatures T, as depicted in Fig. 3.3(a). This result was corroborated by zero-temperature optimization of the spin pattern. Spins within one hexagon are almost FM, the allowed energies for electrons moving on a six-site ring are $-2t_0 \cos 0 = -2t_0$ and $-2t_0 \cos \pi/3 = -t_0$, with twice as many states at $-t_0$, which gives precisely the DOS seen in Fig. 4.2(b). Coupling between the hexagons is AF, but since they occupy a frustrated triangular lattice, see Fig. 3.3(a), perfect AFM order is not possible. The hexagons instead are at an angle of $\approx 2\pi/3$, corresponding to the Yafet-Kittel state [50] well known for the triangular lattice, leading to the signals at $\frac{2}{3}(\pi, 0)$ in $S(\vec{q})$. Thus a geometrically frustrated triangular lattice emerges spontaneously from isotropic, competing interactions on the non-frustrated honeycomb lattice.

For $0.18 \leq J_{AF} \lesssim 0.25$, we find a state consisting of classical dimers. The dimers each consist of two spins aligned in parallel, they cover the lattice in such a way that the neighboring dimers are anti-parallel with respect to each other. In Fig. 3.3(b) and 3.3(c) we show two possible dimer configurations. In this spin texture, the electron kinetic energy reduces to that of uncoupled two-level problems, having only two eigenenergies $\pm t_0$. The DOS is therefore given by $D(\omega) = \delta(\omega - t_0)/2 + \delta(\omega + t_0)/2$, in excellent agreement with MC calculations [see Fig. 4.2(c)]. The dimer state can be understood as a trade-off between the FM ordering and the AFM ordering: the electrons are allowed to populate all the $-t_0$ levels (which is more favorable compared to AFM) and the spins are anti-parallel with respect to two of their nearest neighbors (which is more favorable compared to FM).

Interestingly, the dimer ground state of this quantum system has a macroscopic degeneracy, i.e., there is a macroscopically large number of ways to cover the lattice by dimers such that the neighboring dimers are anti-parallel. One way to see the degeneracy is to start covering lattice rows in Fig. 3.1(b) by dimers. It is easy to see that having fixed the dimer pattern in the 1st row, there are two independent ways of covering each subsequent row, giving $2^{\sqrt{N}-1}$ states for a N-site lattice. The fact that there is thus no long-range order along the y direction of the brick-wall is reflected in $S(\vec{q})$, which becomes finite along *lines* in momentum space, as in compass models [65–68]. In the 2D compass model, different degenerate configurations can be reached by flipping a row of spins. The corresponding $\sqrt{N}$ operators commute with the compass Hamiltonian and thus define an *intermediate* symmetry, i.e., between a local, gauge-like ($\propto e^N$) symmetry and global one (independent of N) [53]. The

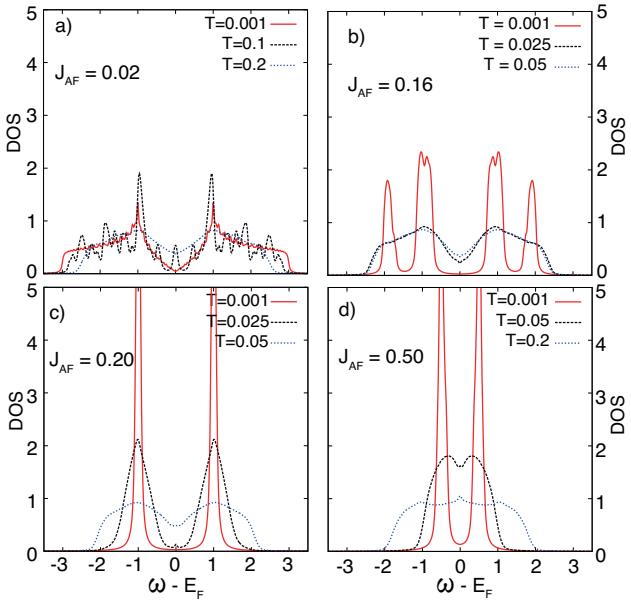

Figure 3.2: (a)-(d) DOS at low, intermediate and high temperatures for different values of J_{AF} ($\gamma = 0.04$). In (a) the $T = 0.001$ curve shows the DOS of free fermions on a honeycomb lattice in the thermodynamic limit. In (d) the $T = 0.001$ curve represents a gapped insulating phase, the seemingly finite DOS at E_F being a broadening effect. Except for the FM phase, all ground states are gapped.

magnetic order parameter that obeys the intermediate symmetry is consequently of nematic type. In the dimer state, the minimal symmetry operations involves translation of all spins in two adjacent zig-zag rows by one lattice spacing, $\sigma_{ij} \mapsto \sigma_{ij+1}$ [σ_{ij} is the spin at site (i, j)]. An example for two dimer configurations connected by such an operation is given in Figs. 3.3(b) and 3.3(c), where the second and third rows were shifted. However, this operator does *not commute with the Hamiltonian* Eq. (4.1), and the intermediate symmetry is thus rather a property that *emerges* in the system's ground state, similar to the case of striped phases at fractional filling in the regime of narrow bandwidth and small Jahn-Teller coupling in a model used for manganites [69]. This intermediate macroscopic degeneracy should lead to a large specific heat at low temperature.

For strong super-exchange coupling, there is a continuous way in which the dimer state can approach the AFM ordered state, captured by a canting angle θ [see Fig.

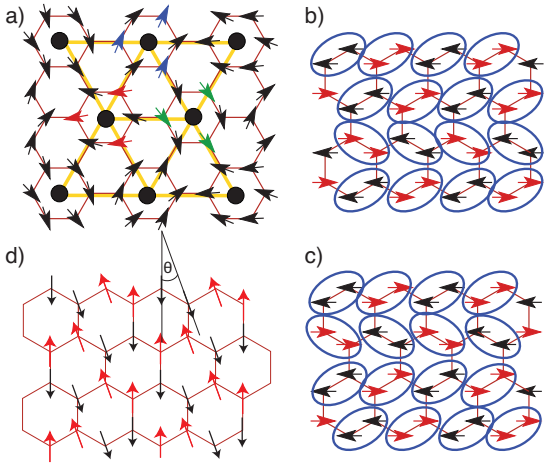

Figure 3.3: (a) Snapshot from MC simulations supplemented by optimization routines showing an emergent triangular lattice (black circles) formed by FM hexagons at $J_{\rm AF} = 0.14$. Spins within each hexagon are almost FM, a small canting angle between groups of three is illustrated by shading. The colored spins illustrate the $2\pi/3$-angle order of the Yafet-Kittel state. Schematic view of, (b)-(c) two dimer states related by a translational symmetry (see text), and (d) a canted dimer state.

3.3(d)], which is the angle between the two spins forming a dimer in the pure dimer phase. The spins remain antiparallel to those of the neighboring canted dimers. In this way, the two-level dimer systems remain uncoupled. The hopping amplitude between the two spins in the dimer is renormalized by the DE mechanism to $t_0 \cos(\theta/2)$. The DOS for a canted dimer state is consequently given by $D(\omega) = \delta(\omega - t_0 \cos(\theta/2))/2 + \delta(\omega + t_0 \cos(\theta/2))/2$, as can indeed be observed in the DOS for $J_{\rm AF} = 0.50$ shown in Fig. 4.2(d). The canted-dimer groundstate has a gap $\propto \cos(\theta/2)$ at the chemical potential, which shrinks as θ approaches π for $J_{\rm AF} \to \infty$. At finite T, the two peaks widen and merge due to thermal spin fluctuations, leading to a metal with reduced band width, see Fig. 4.2(d). This canted state retains the macroscopic degeneracy inherent to the AFM dimer state discussed above – also this ordering is therefore of nematic type.

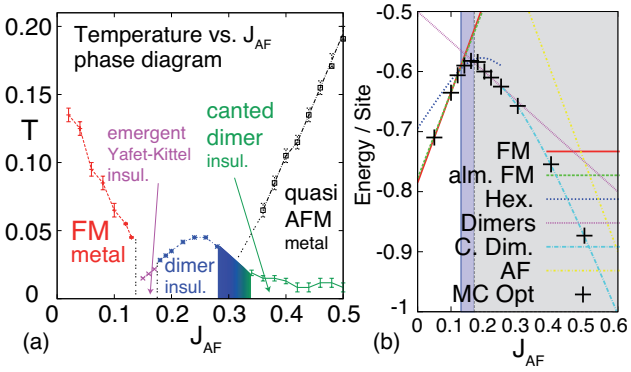

Figure 3.4: (a) T-J_{AF} phase diagram at half-filling obtained by MC for a 12×12 lattice. (b) The energy of the various states: "alm. FM" refers to a spiral with the longest wavelength supported by the lattice, converging to FM in the thermodynamic limit. Similar finite-size effects are reported in doped 1D and 2D lattices [70]. "Hex" denotes the emergent Yafet-Kittel order between hexagons depicted in Fig. 3.3(a), the energy was optimized with respect to the canting angle within the hexagons. "Dimers" and "C. Dim" are the highly degenerate FM and canted dimer states, and "AFM" denotes perfectly AFM order. The black crosses are energies obtained by unbiased MC and a subsequent energy optimization.

3.4 Discussion

Our results are in good agreement with elementary energy considerations. The energy per site varies as $3J_{\rm AF}/2$ and $-J_{\rm AF}/2$ for the FM and the dimer states, respectively. This would imply a phase transition at $J_{AF} \approx 0.15$, the FM state is indeed stable for $J_{\rm AF} \lesssim 0.14$ and the dimers for $J_{\rm AF} \gtrsim 0.18$. In between, the emergent Yafet-Kittel state, with a more complex energy dependence, is favorable, see Fig. 3.4(b). The energy per site for the canted dimer state is $-(2J_{AF} - \cos(\theta)J_{AF} + t_0\cos(\theta/2))/2$. By differentiating with respect to the canting angle θ, one easily obtains that canting becomes favorable for $J_{AF} \geq 0.25$ and that the optimal energy is then given by $-3J_{\rm AF}/2 - t_0^2/(16J_{\rm AF})$. This is reflected in the behavior of the ordering temperature for the dimer state, which starts decreasing at $J_{\rm AF} = 0.25$ [see Fig. 3.4(a)].

The results are summarized in Fig. 3.4. In the finite-T phase diagram Fig. 3.4(a), phase boundaries for the FM and quasi-AFM regions are obtained by determining the inflection point in the $\langle M\rangle(T)$ and $\langle\overline{M}\rangle(T)$ ($\overline{M}$ denotes staggered magnetization) curves. The onset of dimer and other phases is determined by tracking the temperature

dependence of the spin structure factor and the characteristic features in the DOS. Figure 3.4(b) compares the ground-state energies of the various phases and perfectly agrees with the unbiased numerical data, indicating that we have identified the ground states correctly.

In a full quantum treatment of the spin system additional quantum fluctuations can affect the stability of these ordered phases. Here one anticipates the FM building blocks (hexagons and dimers) to be robust as they are stabilized by a substantial DE energy, and the FM state remains an eigenstate of the hexagon (dimer) for quantum spins. The Yafet-Kittel ordering between the large total spins of the hexagons is expected to be more classical, and thus robust, than for $S = 1/2$, where it is found for $T \to 0$ [71]. If one can describe the magnetism of a dimer state by an effective NN AFM Heisenberg model, then this model remains the same if one performs the operation illustrated in Fig. 3.3. The emergent symmetry would thus commute with the effective low-energy Hamiltonian so that the corresponding degeneracies are preserved.

3.5 Conclusions

We conclude that the isotropic double-exchange model with competing super-exchange interactions on the *non-frustrated* honeycomb lattice has an unexpectedly rich phase diagram with exotic magnetic phases. In one of these, FM rings become the essential building blocks, which form a frustrated triangular lattice and are antiferromagnetically coupled. The stabilization of such frustrated spin states on a bipartite honeycomb lattice, without explicit frustration, is so far unique and an example of geometrical frustration emerging from competing interactions. Another novel phase consists of FM dimers ordered antiferromagnetically and has a $2^{\sqrt{N}}$ degeneracy. This is reminiscent of compass models, but in the present case the corresponding symmetry is not a property of the Hamiltonian given a priori, but rather a property that emerges in the systems ground state [65–69]. These phenomena are not only relevant in a theoretical context, immediately raising the question which other models share such features and how further residual interactions might affect the degeneracy, but pertains in particular to honeycomb manganese oxides, which form a promising class of materials to realize these novel types of highly frustrated states harboring macroscopic degeneracies.